

Pion-pion scattering and the timelike pion form factor from $N_f = 2 + 1$ lattice QCD simulations using the stochastic LapH method

John Bulava and Ben Hörz*

School of Mathematics, Trinity College Dublin

Dublin 2, Ireland

E-mail: jbulava@maths.tcd.ie, hoerz@maths.tcd.ie

Brendan Fahy

High Energy Accelerator Research Organization (KEK)

Ibaraki 305-0801, Japan

E-mail: bfahy@post.kek.jp

K. J. Juge

Dept. of Physics, University of the Pacific

Stockton, CA 95211, USA

E-mail: kjuge@pacific.edu

Colin Morningstar

Dept. of Physics, Carnegie Mellon University

Pittsburgh, PA 15213, USA

E-mail: colin_morningstar@cmu.edu

Chik Him Wong

Dept. of Physics, University of Wuppertal

Gaussstrasse 20, D-42119 Germany

E-mail: cwong@uni-wuppertal.de

We report on progress applying the stochastic LapH method to estimate all-to-all propagators required in correlation functions of multi-hadron operators relevant for pion-pion scattering. Large-volume results for $I = 2$ and $I = 1$ pion-pion scattering phase shifts with good statistical precision are obtained from an $N_f = 2 + 1$ anisotropic Wilson clover ensemble with $m_\pi = 240\text{MeV}$. We also present a preliminary determination of the $I = 1$ pion-pion scattering phase shift and timelike pion form factor on an isotropic $N_f = 2 + 1$ flavour ensemble generated by the Coordinated Lattice Simulation (CLS) community effort.

The 33rd International Symposium on Lattice Field Theory

14 -18 July 2015

Kobe International Conference Center, Kobe, Japan

*Combined proceedings from the talks of J. Bulava and B. Hörz.

Lattice QCD simulations are inevitably carried out in finite volume and euclidean time, which complicates scattering calculations [1]. Since most excited hadrons are unstable resonances which appear experimentally as features in scattering cross sections, first-principles calculation of hadron-hadron scattering amplitudes is desirable. The relation between finite-volume two-hadron spectra and infinite-volume elastic scattering amplitudes was formulated by Lüscher [2, 3] more than two decades ago and extended to moving frames in Ref. [4]. However, only recently have algorithmic advances in lattice QCD spectroscopy enabled finite-volume spectra to be calculated efficiently in large volume with light pion masses.

These advances concern the treatment of all-to-all propagators, which are required to give definite momenta to all hadrons and to treat valence-quark-line-disconnected Wick contractions. Laplacian-Heaviside (LapH) quark smearing projects the quark propagator onto the subspace spanned by the lowest-lying N_v eigenmodes of the three-dimensional covariant Laplace operator [5]. Stochastic noise introduced only in the LapH subspace results in more efficient estimators for all-to-all quark propagators compared to noise on the entire lattice [6].

The spatial profile of the LapH subspace projector is approximately Gaussian, as with other quark smearing procedures. In order to maintain a constant physical smearing radius, N_v must increase proportionally to the spatial volume. However, in Ref. [6] it was demonstrated that with a moderate amount of dilution in the LapH subspace, the number of quark matrix inversions can be held constant as the spatial volume is increased without increasing the stochastic estimation error relative to the gauge noise. This enables all-to-all quark propagators to be estimated efficiently in large spatial volumes for a reasonable cost.

The efficient treatment of all-to-all quark propagators in turn enables precision calculation of correlation functions containing multi-hadron interpolating operators with definite momenta and/or disconnected Wick contractions. From these correlation functions, finite-volume energies can be precisely extracted, which then yield elastic scattering amplitudes. The application of these techniques to extract elastic pion-pion scattering amplitudes from large volume ensembles is the subject of this work. Sec. 1 details a first application of the stochastic LapH method to large volume, in which the $I = 1$ and $I = 2$ elastic pion-pion scattering phase shifts are calculated. With an eye toward larger, finer lattices at lighter pion masses, Sec. 2 presents a preliminary calculation of the $I = 1$ scattering phase shift and timelike pion form factor on an ensemble generated through the Coordinated Lattice Simulations (CLS) community effort.

1. $I = 1$ and $I = 2$ phase shifts from a large-volume anisotropic lattice

For a first large-volume application of the stochastic LapH method, we employ an anisotropic lattice regularization, in which the spatial lattice spacing (a_s) is larger than the temporal one (a_t). The renormalized anisotropy $\xi_R = \frac{a_s}{a_t}$ is defined by demanding that pions satisfy the correct (continuum) dispersion relation

$$(a_t E_\pi)^2 = (a_t m_\pi)^2 + \left(\frac{2\pi a_s}{\xi_R L} \right)^2 \mathbf{d}^2, \quad (1.1)$$

where $\mathbf{d} \in \mathbb{Z}^3$ is the quantized finite-volume momentum. Details on the anisotropic ensemble used here are found in Tab. 1.

$(L/a_s)^3 \times (T/a_t)$	$m_\pi(\text{MeV})$	$a_t(\text{fm})$	ξ_R	$m_\pi L$	N_{cfg}
$32^3 \times 256$	240	0.035	3.4418(94)	4.3	412

Table 1: Details for the anisotropic $N_f = 2 + 1$ gauge configurations used here. For a complete discussion of the ensemble generation and scale setting, see Ref. [7]. For definition of the LapH subspace and specification of dilution schemes, see Ref. [6].

The anisotropy is crucial in defining the center-of-mass momentum (discussed later), and thus care must be taken in its determination. We employ two different methods which are consistent within statistical errors. In the first we calculate $a_t E_\pi$ for all pions with $\mathbf{d}^2 \leq 5$ on $N_b = 800$ identical bootstrap samples of the corresponding correlation functions using correlated χ^2 fits. We then perform correlated χ^2 fits on each bootstrap sample to Eq. 1.1 to obtain ξ_R . Our second determination of ξ_R simultaneously fits all of these correlation functions to obtain ξ_R directly.

In order to calculate elastic scattering phase shifts, we require correlation functions containing two-pion interpolating operators which transform irreducibly according to the lattice symmetries. In particular, we require such correlation functions at various total momenta, and construct appropriate operators which transform irreducibly under the corresponding little groups according to Ref. [8]. While this operator construction procedure can be used to construct spatially-extended operators with gauge-covariantly displaced quark fields (which are ideal for high-lying resonance states), we employ only single-site hadron operators in this work.

In order to extract the finite-volume energies in each irrep we evaluate a matrix of correlation functions $C_{ij}(t) = \langle O_i(t) \bar{O}_j(0) \rangle$ and solve the generalized eigenvalue problem (GEVP)

$$C(t_d)v(t_0, t_d) = \lambda(t_0, t_d)C(t_0)v(t_0, t_d) \quad (1.2)$$

for a single (t_0, t_d) . The eigenvectors $\{v_n(t_0, t_d)\}$ from this diagonalization define ‘optimal’ interpolating operators [9] whose correlation matrix $\hat{C}_{ij}(t) = \langle \mathcal{O}_i(t) \bar{\mathcal{O}}_j(0) \rangle = (v_i(t_0, t_d), C(t)v_j(t_0, t_d))$ is mostly diagonal. In order to get a preliminary idea of the spectrum, we perform single exponential fits to the diagonal elements of this rotated correlation matrix to extract the energies, taking care to vary (t_0, t_d) to ensure that any systematic error associated with the off-diagonal elements of the rotated correlation matrix is smaller than the statistical one. We find that generally the variation of the GEVP parameters has little effect on the extracted energies. The fitting range $[t_{\min}, t_{\max}]$ is chosen by fixing $t_{\max} = 38a_t$ and varying t_{\min} until a suitable χ^2 is achieved and a plateau is evident. Examples of such t_{\min} plots are shown in Fig. 1 which illustrate both the quality of the plateaux and insensitivity to the GEVP parameters.

In addition to finite-volume energies, we can use GEVP eigenvectors to estimate the overlaps $Z_{in} = |\langle 0 | \hat{O}_i | n \rangle|^2$ between our operators and the finite-volume Hamiltonian eigenstates. We estimate these overlaps by constructing the ratio

$$Z_{in}(t) = \left| \frac{\sum_j C_{ij}(t) v_{nj}(t_0, t_d)}{e^{-\frac{E_n}{2}t} \sqrt{\hat{C}_{nn}(t)}} \right|^2, \quad (1.3)$$

where E_n is the fitted energy, and taking $t = 20a_t$.

The $I = 1$ finite-volume spectra in irreps where an infinite-volume $J^{PG} = 1^{-+}$ state appears are shown in Fig. 2. There we show center-of-mass energies $E_{\text{cm}} = \sqrt{E^2 - \mathbf{P}^2}$, with $\mathbf{P} = \frac{2\pi}{L}\mathbf{d}$, in

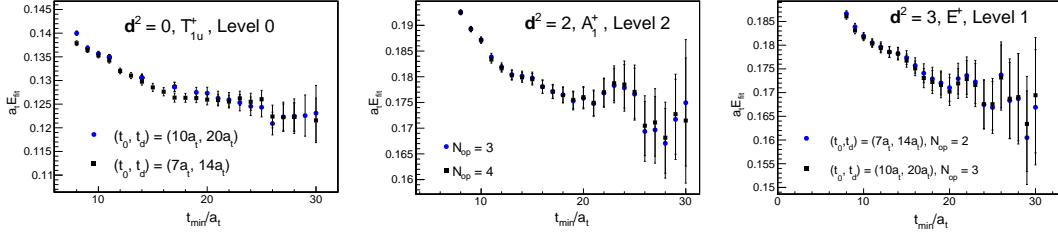


Figure 1: Representative t_{\min} plots from exponential fits to diagonal elements of the rotated correlation matrices. Each plot shows results from two different choices for the GEVP parameters.

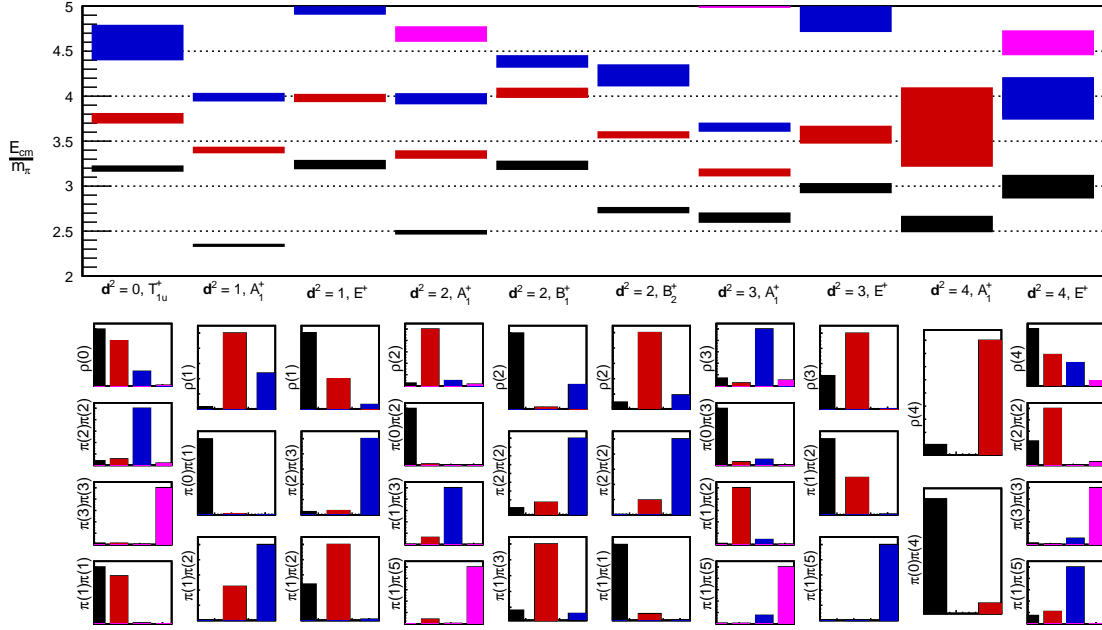


Figure 2: $I = 1$ center-of-mass energies (upper panel) for each irrep together with the overlaps of each interpolator. Each column corresponds to an irrep, and the bar graphs below show relative overlaps of each interpolating operator onto the (color-coded) finite-volume Hamiltonian eigenstates.

units of m_π as well as overlaps onto our interpolators. As the ρ meson is present in these irreps, we employ local single-meson operators (denoted $\rho(\mathbf{d}^2)$) as well as two-pion operators, which are denoted $\pi(\mathbf{d}_1^2)\pi(\mathbf{d}_2^2)$ where $\mathbf{d}^2 = (\mathbf{d}_1 + \mathbf{d}_2)^2$. Correlation functions with equivalent total momenta are averaged for each \mathbf{d}^2 .

A clear picture emerges from these energies and overlaps. It is only two-pion interpolating operators which have significant overlap with states far below $\frac{E_{\text{cm}}}{m_\pi} \approx 3.2$, while single- ρ interpolators have overlap for states with energies at or above this value. Due to G -parity, the lowest-lying inelastic threshold is at $E_{\text{cm}} = 4m_\pi$. While we are able to precisely extract energies near and above this threshold, they cannot be used to extract infinite-volume scattering information. Although extensions of the Lüscher formula above three-hadron thresholds has been developed [10, 11, 12, 13], a rigorous treatment of four-hadron thresholds is still lacking.

In order to obtain elastic scattering phase shifts, we first define the kinematic quantities

$$E_{\text{cm}} = \sqrt{E^2 - \mathbf{P}^2}, \quad \gamma = \frac{E}{E_{\text{cm}}}, \quad \mathbf{q}_{\text{cm}}^2 = \frac{1}{4}E_{\text{cm}}^2 - m_\pi^2, \quad u^2 = \frac{L^2 \mathbf{q}_{\text{cm}}^2}{(2\pi)^2}, \quad (1.4)$$

where E is the fitted two-hadron energy. Generally, the relation between these quantities and the infinite-volume scattering matrix takes the form $\det \{1 + F^{(\mathbf{d}, \gamma)}(u^2)[S(E_{\text{cm}}) - 1]\} = 0$, where F is a known kinematic function and S is the infinite-volume scattering matrix. This relation holds up to corrections which are exponential in the volume and the determinant is taken over the usual (ℓ, m) indices of partial waves, in which F is non-diagonal.

For this work we ignore higher partial waves. Precisely, this means neglecting $\ell \geq 3$ partial waves in $I = 1$ p -wave scattering and $\ell \geq 2$ partial waves in $I = 2$ s -wave scattering. After applying this approximation and block-diagonalizing in lattice irreps, the above relation takes the particularly simple form

$$q_{\text{cm}}^{2\ell+1} \cot \delta_\ell = -q_{\text{cm}}^{2\ell+1} \phi^{(\mathbf{d}, \gamma, \Lambda)}(u^2) \quad (1.5)$$

for each finite-volume irrep Λ . The functions $\phi^{(\mathbf{d}, \gamma, \Lambda)}(u^2)$ involve Rummukainen-Gottlieb-Lüscher shifted zeta functions ($Z_{lm}^{(\mathbf{d}, \gamma)}(u^2)$) and are given in e.g. Ref. [14] for $I = 1$, $\ell = 1$. For $I = 2$, Eq. 1.5 takes the even simpler form

$$q_{\text{cm}} \cot \delta_0(q_{\text{cm}}^2) = \frac{2}{\gamma L \sqrt{\pi}} Z_{00}^{(\mathbf{d}, \gamma)}(u^2) \quad (1.6)$$

for both the A_{1g}^+ and A_1^+ irreps used in this work. It should be noted that near the two-pion threshold $q_{\text{cm}}^{2\ell+1} \cot \delta_\ell$ is analytic and thus Eq. 1.5 is valid for also for negative q_{cm}^2 . In order to efficiently evaluate these zeta functions we employ a method described in Ref. [15] which agrees with our implementation of Appendix A in Ref. [14].

While the single-exponential fits discussed above provide preliminary spectra, the center-of-mass momentum and thus the scattering phase shifts are very sensitive to these energies. For two-hadron dominated levels, the energies will be very close to their non-interacting values. Therefore, for these levels it is beneficial to perform fits to the ratio of two and single-hadron correlators (as in Ref. [16] but here generalized to arbitrary momenta)

$$R(t) = \frac{\langle \hat{\mathcal{O}}_{\mathbf{d}_1^2, \mathbf{d}_2^2}(t) \bar{\mathcal{O}}_{\mathbf{d}_1^2, \mathbf{d}_2^2}(0) \rangle}{\langle O_{\mathbf{d}_1}(t) \bar{O}_{\mathbf{d}_1}(0) \rangle \langle O_{\mathbf{d}_2}(t) \bar{O}_{\mathbf{d}_2}(0) \rangle}, \quad (1.7)$$

where $\hat{\mathcal{O}}_{\mathbf{d}_1^2, \mathbf{d}_2^2}$ is a optimized operator for an eigenstate dominated by individual pions with momenta of magnitude \mathbf{d}_1^2 and \mathbf{d}_2^2 , respectively. The $O_{\mathbf{d}}$ are single-pion operators with momentum \mathbf{d} . Single exponential fits to these ratios directly yield this energy difference, and typically have less excited state contamination than ordinary single exponential fits. However, the excited state contamination in such fits may not be monotonically decreasing, which can complicate the identification of the plateau region in some cases. Another method to better resolve differences between the two- and single-hadron energies is to perform simultaneous fits to the two hadron correlators included in the ratio of Eq. 1.7. While both methods yield consistent results, we quote values from the simultaneous fits, as they result in more conservative statistical errors.

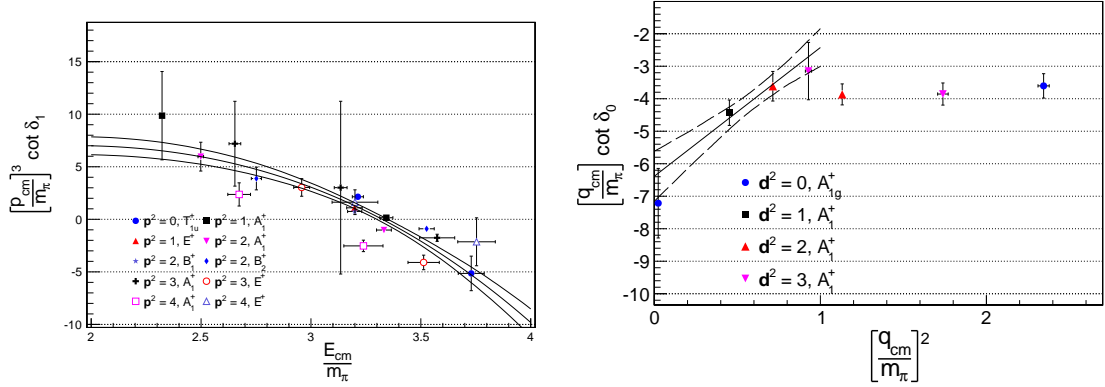


Figure 3: The $I = 1$ p -wave scattering phase shift (left) and $I = 2$ s -wave phase shift (right) together with fits to $q_{cm}^{2\ell+1} \cot \delta_\ell$ described in the text.

The resultant scattering phase shifts are shown in Fig. 3 for both $I = 1$ and $I = 2$, together with fits to $q_{cm}^{2\ell+1} \cot \delta_\ell$. Care must be taken to treat the correlation between x - and y -errors as well as among the data points in these fits. Upon every call to the correlated χ^2 function, we estimate the necessary covariance matrix using the $N_b = 800$ bootstrap samples of these secondary observables. The minimization is performed on each bootstrap sample, where bootstrap replica of the means are used together with the covariance matrix to construct the correlated χ^2 . For $I = 1$ p -wave scattering, we fit to a relativistic Breit-Wigner form

$$\left(\frac{q_{cm}}{m_\pi}\right)^3 \cot \delta_1 = \left(\frac{m_\rho^2}{m_\pi^2} - \frac{E_{cm}^2}{m_\pi^2}\right) \frac{6\pi E_{cm}}{g_{\rho\pi\pi}^2 m_\pi} \quad (1.8)$$

and obtain

$$g_{\rho\pi\pi} = 6.16(36), \quad \frac{m_\rho}{m_\pi} = 3.324(24), \quad \frac{\chi^2}{d.o.f.} = 1.43 \quad (1.9)$$

where the coupling is in good agreement with the experimental value. For $I = 2$ s -wave scattering, we employ the NLO effective range expansion to the points at low momenta $q_{cm} \leq m_\pi$

$$\left(\frac{q_{cm}}{m_\pi}\right) \cot \delta_0 = \frac{1}{m_\pi a_0} + \frac{1}{2}(m_\pi r) \left(\frac{q_{cm}}{m_\pi}\right)^2 \quad (1.10)$$

and obtain

$$m_\pi a_0^{I=2} = -0.157(19), \quad m_\pi r = 7.9(2.4), \quad \chi^2/d.o.f. = 0.61. \quad (1.11)$$

The JLab group [17] has recently calculated the $I = 1$ p -wave phase shift on this same ensemble using the distillation method of Ref. [5]. While their results are more precise than those quoted here, significantly more Dirac matrix inversions are required. Using the notation of Ref. [6], we employ (TF, SF, LI8) dilution for fixed quark lines and (TI16, SF, LI8) for relative ones. Our use of five fixed and two relative lines (with eight source times) results in $N_D = 2304$ Dirac matrix inversions for each gauge configuration, while Ref. [17] requires $N_D = 393216$ for the distillation method.

$(L/a)^3 \times (T/a)$	$m_\pi(\text{MeV})$	$a(\text{fm})$	$m_\pi L$	N_{cfg}
$48^3 \times 128$	280	0.065	4.3	1710

Table 2: Details for the isotropic $N_f = 2 + 1$ gauge configurations used here. For a complete discussion of the ensemble generation and preliminary scale setting, see Ref. [18].

2. $I = 1$ phase shifts and the timelike pion form factor on a CLS ensemble

Motivated by the efficacy of the stochastic LapH method in the large-volume calculation described in Sec. 1, we now employ it to isotropic $N_f = 2 + 1$ ensembles generated within the CLS community effort [18]. These ensembles have a variety of lattice spacings, physical volumes, and pion masses enabling an assessment of these systematic errors. As a first step in this direction, here we use a single ensemble (the N200) which is described in Tab. 2.

Rather than the periodic (anti-periodic) temporal boundary conditions for bosons (fermions) which are typically employed in the lattice QCD simulations, these ensembles use ‘open’ temporal boundary conditions [19] which improve the scaling of the exponential autocorrelation time τ_{exp} as the continuum limit is approached. This means source and sink times must be chosen carefully in order to avoid boundary effects. Based on the observables considered in Refs. [18, 20] and on the behavior of the LapH eigenvalues, we use $t_0 = T/4 = 32a$.

In the gauge-covariant 3-D Laplace operator used to define the LapH subspace we stout smear [21] the gauge links with parameters $(\rho, n_\rho) = (0.1, 36)$. We choose a LapH cutoff $\sigma_s \approx 1\text{GeV}$ which results in a cutoff eigenvalue of $(a\sigma_s)^2 \approx 0.11$ and $N_v = 192$. The physical volume is somewhat smaller on this lattice compared to the anisotropic ensemble of Sec. 1, so a reduced N_v is expected. We employ the same (TF, SF, LI8) dilution scheme for fixed lines, but for relative lines use (TI8, SF, LI8) as the temporal lattice spacing is larger. We use four independent fixed quark lines, a single relative line, and one source time $t_0 = 32a$. The $N_D = 384$ Dirac matrix inversions per configuration are performed using the DFL-SAP-GCR solver [22] implemented in `openQCD`¹, which we have integrated into the stochastic LapH codebase. The results from these inversions are projected onto the LapH subspace and stored for later use in other calculations, such as Ref. [23]. Finally, these ensembles employ RHMC and twisted mass re-weighting, and we multiply all primary observables by the corresponding re-weighting factors.

The renormalization and $O(a)$ improvement of composite operators is simplified on an isotropic lattice. Furthermore, the regularization employed by these CLS ensembles is well studied and many renormalization and improvement coefficients have been previously determined. Therefore, in addition to applying the methods of Sec. 1 to calculate the $I = 1$ p -wave scattering phase shift, we also calculate a matrix element of the vector current with two-pion states. The simplest such matrix element of phenomenological relevance is the timelike pion form factor. As before we are restricted to the elastic region which, for this ensemble is $2m_\pi \leq E_{\text{cm}} \leq 2m_K$. In this region the timelike pion form factor $|F_\pi(E_{\text{cm}})|^2$ can be defined as [24]

$$R(s) \equiv \frac{\sigma(e^+e^- \rightarrow \text{hadrons})}{4\pi\alpha(s)^2/(3s)} = \frac{1}{4} \left(1 - \frac{4m_\pi^2}{s}\right)^{\frac{3}{2}} |F_\pi(\sqrt{s})|^2, \quad (2.1)$$

¹<http://luscher.web.cern.ch/luscher/openQCD/>

where the denominator in $R(s)$ is the tree-level cross section $\sigma(e^+e^- \rightarrow \mu^+\mu^-)$ for $s = E_{\text{cm}}^2 \gg m_\mu^2$. Effectively, this form factor describes QCD corrections to the coupling of a (virtual) photon to two pions. It is phenomenologically relevant because of (e.g.) its relation to the low-energy contribution to the hadronic vacuum polarization (HVP) $\Pi(Q^2)$. For spacelike four-momentum transfer Q^2 , the once-subtracted dispersion relation

$$\Pi(0) - \Pi(Q^2) = Q^2 \int_0^\infty ds \frac{\rho(s)}{s(s+Q^2)}, \quad \rho(s) = \frac{R(s)}{12\pi^2} \quad (2.2)$$

expresses the HVP in terms of $R(s)$. Typically, this dispersion relation is not used in lattice QCD calculations of the HVP which is instead calculated directly from current-current correlation functions. Furthermore, the relation between $R(s)$ and $|F_\pi(E_{\text{cm}})|^2$ given in Eq. 2.1 is valid only in the elastic region, while the integral in Eq. 2.2 is unbounded from above. However, direct lattice calculations of the HVP require fully disconnected Wick contractions (which are typically ignored), and suffer from large statistical errors and finite-volume effects in the low- Q^2 region [25]. Therefore, a ‘hybrid’ determination which combines lattice data from both $\Pi(Q^2)$ and $|F_\pi(E_{\text{cm}})|^2$ may be the best approach².

In analogy with earlier work by Lellouch and Luscher [26], a relation between the infinite-volume $|F_\pi(E_{\text{cm}})|^2$ and finite-volume matrix elements (up to exponential finite-volume corrections) was derived by Meyer in Ref. [27]

$$|F_\pi(E_{\text{cm}})|^2 = g^{(\mathbf{d},\Lambda)}(\gamma) \left(u \frac{d\phi^{(\mathbf{d},\Lambda)}(u^2)}{du} + q_{\text{cm}} \frac{\partial \delta_1(q_{\text{cm}})}{\partial q_{\text{cm}}} \right) \frac{3\pi E_{\text{cm}}^2}{2q_{\text{cm}}^5} |A^{(\mathbf{d},\Lambda)}|^2, \quad (2.3)$$

$$g^{(\mathbf{d},\Lambda)}(\gamma) = \begin{cases} 1/\gamma & \text{if } \Lambda = A_1 \\ \gamma & \text{else} \end{cases},$$

where $\phi^{(\mathbf{d},\Lambda)}(u^2)$ is given in Eq. 1.5 and

$$A^{(\mathbf{d},\Lambda)} = \langle 0 | V^{(\mathbf{d},\Lambda)} | \mathbf{d} \Lambda n \rangle \quad (2.4)$$

is a finite-volume matrix element involving an $I = 1$ two-pion state with total momentum \mathbf{d} in irrep Λ below inelastic threshold. While this relation was derived only for total zero momentum in Ref. [27], it may be straight-forwardly extended to non-zero total momentum using the argumentation of Ref. [28]. A proof-of-principle application of this relation was performed recently in Ref. [29] while a similar matrix element is calculated in Ref. [30].

Since we work in the isospin limit, the electromagnetic current $\hat{f}_i^{\text{em}} = \frac{2}{3}\bar{u}\gamma_i u - \frac{1}{3}\bar{d}\gamma_i d - \dots$ is replaced by the isospin current

$$V_i^a = \bar{\psi} \gamma_i \frac{\tau^a}{2} \psi, \quad \psi = \begin{pmatrix} u \\ d \end{pmatrix}, \quad (2.5)$$

where τ^a is an $SU(2)$ generator. Furthermore, we project this current onto finite-volume irreps by defining $V^{(\mathbf{d},\Lambda)} = b_i^{(\mathbf{d},\Lambda)} V_i$. The vectors $\mathbf{b}^{(\mathbf{d},\Lambda)}$ are given in Tab. 3 for all irreps used in this work. In order to obtain the derivative of the p -wave phase shift required in Eq. 2.3, we first perform the

²We thank Harvey Meyer for clarifying this point.

Reference momentum \mathbf{d}	Irrep Λ	\mathbf{b}
[000]	T_{1u}	(1,0,0)
[00n]	A_1	(0,0,1)
	E	(0,1,0)
[0nn]	A_1	$\frac{1}{\sqrt{2}}$ (0,1,1)
	B_1	(1,0,0)
	B_2	$\frac{1}{\sqrt{2}}$ (0,-1,1)
[nnn]	A_1	$\frac{1}{\sqrt{3}}$ (1,1,1)
	E	$\frac{1}{\sqrt{2}}$ (1,-1,0)

Table 3: Linear combinations of components of the vector current such that $V^{(\mathbf{d},\Lambda)} = b_i^{(\mathbf{d},\Lambda)} V_i$ transforms irreducibly according to the irrep Λ .

complete phase shift analysis and parametrize the energy dependence of δ_1 using the Breit-Wigner form of Eq. 1.8. The derivative is then evaluated on each bootstrap sample and taken together with bootstrap samples of the current matrix elements of Eq. 2.4 to obtain samples of $|F_\pi(E_{\text{cm}})|^2$.

In order to obtain the current matrix elements in Eq. 2.4, we must evaluate correlation functions of the form

$$D_i(t) = \langle V^{(\mathbf{d},\Lambda)}(t_0+t) \bar{O}_i^{(\mathbf{d},\Lambda)}(t_0) \rangle, \quad (2.6)$$

where the $\{O_i^{(\mathbf{d},\Lambda)}\}$ are interpolators used in the GEVP of Eq. 1.2. In order to ensure an $O(a^2)$ approach to the continuum limit, the currents $V^{(\mathbf{d},\Lambda)}$ are linear combinations of the renormalized, $\mathcal{O}(a)$ -improved local vector current $(V_R)_\mu$ defined as [31]

$$(V_R)_\mu^a = Z_V(1 + b_V am_q)\{V_\mu^a + ac_V \tilde{\partial}_V T_{\mu\nu}^a\}, \quad (2.7)$$

where Z_V , b_V , and ac_V are renormalization and improvement coefficients, am_q the bare quark mass in lattice units, $T_{\mu\nu}^a = i\bar{\psi}\sigma_{\mu\nu}\frac{\tau^a}{2}\psi$, and $\tilde{\partial}_V$ the symmetrized lattice derivative. A preliminary determination of the renormalization coefficient Z_V for the CLS lattice regularization has been provided in Ref. [32], while b_V , and ac_V are calculated to 1-loop in Ref. [33]. For this preliminary work, we substitute the unrenormalized PCAC mass am_{PCAC} for am_q which holds at tree level, so that $O(a)$ improvement is formally implemented only at this order. However, this effect is suppressed by the small quark mass.

In the stochastic LapH framework interpolators are built from quark fields projected onto the LapH subspace, while quark fields appearing in the current are local. However, this can be easily accommodated by forming the meson functions in Eq. 32 of Ref. [6] with quark sinks which are not projected into the LapH subspace. The unprojected ‘current’ functions are otherwise completely analogous to the meson functions in the construction of correlators but are calculated immediately after the Dirac matrix inversions but before the sinks are projected and written out to disk. In practice, correlation functions required for the matrix elements

$$A_n^{(0)} = \langle 0|V^{(\mathbf{d},\Lambda)}|\mathbf{d}\Lambda n\rangle, \quad A_n^{(1)} = \langle 0|b_i^{(\mathbf{d},\Lambda)} \tilde{\partial}_V T_{i\nu}^a|\mathbf{d}\Lambda n\rangle \quad (2.8)$$

are calculated and analyzed separately.

We turn now to extraction of the matrix elements given Eq. 2.8. In analogy with our procedure for the energies, we measure the correlation functions of Eq. 2.6 and with the GEVP eigenvectors form their ‘optimized’ counterparts $\hat{D}_i(t) = (D(t), v_i(t_0, t_d))$, where the inner product is taken over the GEVP indices. Up to GEVP corrections (treated as a systematic error as described in the previous section) these optimized correlation functions have the large-time behavior

$$\lim_{t \rightarrow \infty} \hat{D}_i(t) = \langle 0 | V^{(\mathbf{d}, \Lambda)} | \mathbf{d} \Lambda i \rangle \langle \mathbf{d} \Lambda i | \bar{O}_i^{(\mathbf{d}, \Lambda)} | 0 \rangle \times e^{-E_i^{(\mathbf{d}, \Lambda)}(t-t_0)}. \quad (2.9)$$

This suggests three different ratios which tend to the matrix elements of interest:

$$R_1^{(i)}(t) = \frac{\hat{D}_i(t)}{\hat{C}_{ii}^{\frac{1}{2}}(t) e^{-\frac{1}{2} E_i(t-t_0)}}, \quad R_2^{(i)}(t) = \frac{\hat{D}_i(t) \langle \mathbf{d} \Lambda n | \bar{O}_i^{(\mathbf{d}, \Lambda)} | 0 \rangle}{\hat{C}_{ii}(t)}, \quad R_3^{(i)}(t) = \frac{\hat{D}_i(t)}{\langle \mathbf{d} \Lambda n | \bar{O}_i^{(\mathbf{d}, \Lambda)} | 0 \rangle e^{-E_i(t-t_0)}}, \quad (2.10)$$

where the overlaps and energies appearing in these expressions are obtained from fits to the diagonal elements of the rotated correlation matrix. The value of the matrix element is taken to be a plateau average of the ratio over a suitable region. Alternatively, simultaneous fits to $\hat{C}_{ii}(t)$ and $\hat{D}_i(t)$ may also be used to extract the desired matrix elements. Generally we find that all four of these different determinations yield results which are consistent within statistical errors for fit ranges in the plateau region.

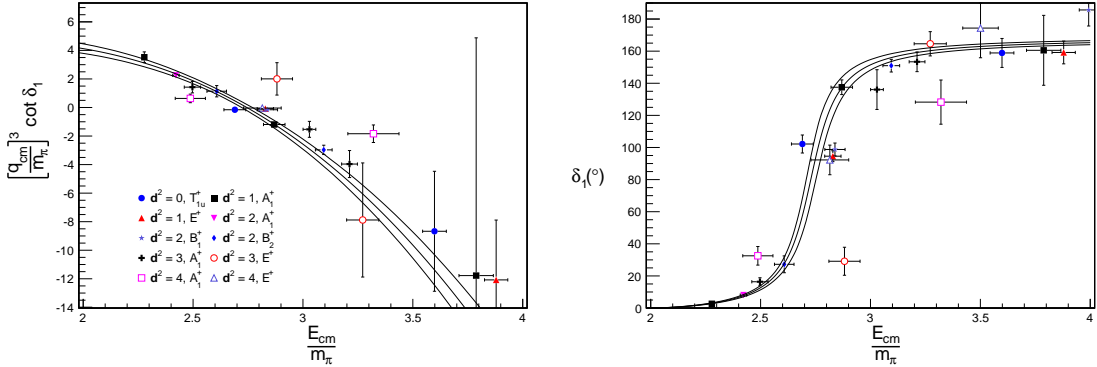


Figure 4: The p -wave scattering phase shift on the N200 CLS lattice. Shown are $q_{\text{cm}}^3 \cot \delta_1$ (left) and δ_1 (right) together with a Breit-Wigner fit to $q_{\text{cm}}^3 \cot \delta_1$. The resultant fit parameters are given in the text. The lowest inelastic threshold is at $2m_K \approx 3.2m_\pi$. Points above this threshold are shown on the graphs but not included in the fit.

Our results from the phase shift determination on this lattice are shown in Fig. 4. As mentioned above, the lowest inelastic threshold in this channel is due to two kaons at $2m_K \approx 3.2m_\pi$. Although we have a number of energy levels above this threshold, they are not included in the final analysis but shown for illustration. As before, we fit $q_{\text{cm}}^3 \cot \delta_1$ to the Breit-Wigner form of Eq. 1.8 which gives

$$g_{p\pi\pi} = 5.68(24), \quad \frac{m_p}{m_\pi} = 2.745(24), \quad \frac{\chi^2}{d.o.f.} = 1.20 \quad (2.11)$$

which is somewhat lower than the experimental value of $g_{\rho\pi\pi}$. The Breit-Wigner parametrization of the phase shift in Eq. 2.3 together with the matrix elements $A^{(0)}$, $A^{(1)}$ and renormalization/improvement coefficients of Eq. 2.7 enables the extraction $|F_\pi(E_{\text{cm}})|^2$, which is shown in Fig. 5. Also shown in that figure is the ratio of the matrix element appearing in the $O(a)$ term over the leading order one. We see that this $O(a)$ matrix element grows from $\sim 10\%$ of the leading one at low momenta to $\sim 30\%$ at our largest momentum. Due to the small 1-loop value of ac_V , this term therefore has no significant effect on our final results. However, non-perturbative determinations of these improvement coefficients can be considerably larger than the 1-loop value [34] possibly increasing the influence of this term to the few-percent level. In future work, an alternative calculation which employs the point-split vector current will give an additional handle on the magnitude of these $O(a)$ effects.

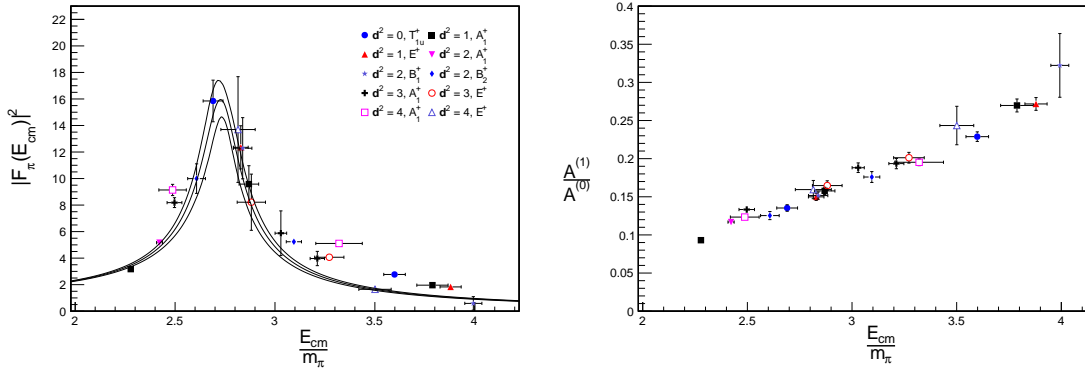


Figure 5: The timelike pion form factor together with the expected Gounaris-Sakurai parametrization using the previously-calculated m_ρ and $g_{\rho\pi\pi}$ (left). The ratio of the matrix element which contributes at $O(a)$ over the leading order one is shown on the right for each of the form factor data points.

Also shown in Fig. 5 is the Gounaris-Sakurai parametrization of $|F_\pi(E_{\text{cm}})|^2$ which (using the notation of Ref. [35]) is

$$F_\pi^{GS}(\sqrt{s}) = \frac{f_0}{q_{\text{cm}}^2 h(\sqrt{s}) - q_\rho^2 h(m_\rho) + b(q_{\text{cm}}^2 - q_\rho^2) - \frac{q_{\text{cm}}^3}{\sqrt{s}} i}, \quad (2.12)$$

$$b = -h(m_\rho) - \frac{24\pi}{g_{\rho\pi\pi}^2} - \frac{2q_\rho^2}{m_\rho} h'(m_\rho), \quad f_0 = -\frac{m_\pi^2}{\pi} - q_\rho^2 h(m_\rho) - b \frac{m_\rho^2}{4}, \quad h(\sqrt{s}) = \frac{2}{\pi} \frac{q_{\text{cm}}}{\sqrt{s}} \ln \left(\frac{\sqrt{s} + 2q_{\text{cm}}}{2m_\pi} \right),$$

where q_ρ is the center-of-mass momentum at the resonance energy. The curve shown in Fig. 5 is not a fit but a ‘prediction’ using the values of m_ρ and $g_{\rho\pi\pi}$ obtained from the phase shift analysis. We see that this GS model fits our data rather well.

3. Conclusion

A first large-volume application of the stochastic LapH method to calculate pion-pion scattering on an anisotropic lattice has been performed. This results in a good precision for both the $I = 1$ and $I = 2$ the phase shift and improved momentum resolution due to the large volume. While the energies differ significantly from their non-interacting values in the $I = 1$ p -wave irreps, stochastic

LapH is sufficiently precise to resolve the differences for $I = 2$ s -wave scattering phase shift as well. The fewer points below inelastic threshold here are due to the reduced number of irreps in which the s -wave contributes. A first look at scattering in the final isospin combination ($I = 0$) is underway, but complicated by both ‘annihilation’ Wick contractions and the need for a vev subtraction when $\mathbf{d} = 0$.

Motivated by this success on the anisotropic lattice, we have started to apply these techniques to isotropic lattices with lighter pion masses and smaller lattice spacings generated by the CLS community effort. This work reports on a first preliminary calculation of the $I = 1$ p -wave scattering phase shift on a single $48^2 \times 128$ ensemble with $m_\pi = 280\text{MeV}$ and $a = 0.064\text{fm}$. Using considerably fewer Dirac matrix inversions on this ensemble compared with the anisotropic one yields results for m_ρ and $g_{\rho\pi\pi}$ with comparable statistical precision. Apart from the scattering phase shift, we also calculate the timelike pion form-factor, which is related to the hadronic vacuum polarization at low four-momentum transfer. Given the moderate number of inversions required, we plan to increase our current level of statistics for this form factor by using an additional source time. Furthermore, while we average over equivalent orientations of the total momentum \mathbf{d} in calculation of the correlation functions used for δ_1 , we have not done so for those used for $|F_\pi(Q^2)|^2$. Preliminary tests indicate that this averaging has a significant impact on the precision of the form factor and it will be performed on the additional source time, possibly resulting in a significant reduction in the statistical errors. Finally, calculations of the scattering phase shift and timelike pion form factor on additional CLS ensembles are underway.

Acknowledgments

BH is supported by Science Foundation Ireland under Grant No. 11/RFP/PHY3218. CJM acknowledges support from the U.S. NSF under award PHY-1306805 and through TeraGrid/XSEDE resources provided by TACC, SDSC, and NICS under grant number TG-MCA07S017. The authors wish to acknowledge the DJEI/DES/SFI/HEA Irish Centre for High-End Computing (ICHEC) for the provision of computational facilities and support. The CLS consortium also acknowledges PRACE for awarding access to resource FERMI based in Italy at CINECA, Bologna and to resource SuperMUC based in Germany at LRZ, Munich. Furthermore, this work was supported by a grant from the Swiss National Supercomputing Centre (CSCS) under project ID s384. We are grateful for the support received by the computer centers.

References

- [1] L. Maiani and M. Testa, *Final state interactions from Euclidean correlation functions*, *Phys. Lett.* **B245** (1990) 585–590.
- [2] Lüscher, Martin, *Two particle states on a torus and their relation to the scattering matrix*, *Nucl. Phys.* **B354** (1991) 531–578.
- [3] Lüscher, Martin, *Signatures of unstable particles in finite volume*, *Nucl. Phys.* **B364** (1991) 237–254.
- [4] K. Rummukainen and S. A. Gottlieb, *Resonance scattering phase shifts on a nonrest frame lattice*, *Nucl. Phys.* **B450** (1995) 397–436, [[hep-lat/9503028](#)].

- [5] **Hadron Spectrum** Collaboration, M. Peardon, J. Bulava, J. Foley, C. Morningstar, J. Dudek, R. G. Edwards, B. Joo, H.-W. Lin, D. G. Richards, and K. J. Juge, *A Novel quark-field creation operator construction for hadronic physics in lattice QCD*, *Phys. Rev.* **D80** (2009) 054506, [[arXiv:0905.2160](#)].
- [6] C. Morningstar, J. Bulava, J. Foley, K. J. Juge, D. Lenkner, M. Peardon, and C. H. Wong, *Improved stochastic estimation of quark propagation with Laplacian Heaviside smearing in lattice QCD*, *Phys. Rev.* **D83** (2011) 114505, [[arXiv:1104.3870](#)].
- [7] **Hadron Spectrum** Collaboration, H.-W. Lin et al., *First results from 2+1 dynamical quark flavors on an anisotropic lattice: Light-hadron spectroscopy and setting the strange-quark mass*, *Phys. Rev.* **D79** (2009) 034502, [[arXiv:0810.3588](#)].
- [8] C. Morningstar, J. Bulava, B. Fahy, J. Foley, Y. Jhang, et al., *Extended hadron and two-hadron operators of definite momentum for spectrum calculations in lattice QCD*, *Phys. Rev.* **D88** (2013), no. 1 014511, [[arXiv:1303.6816](#)].
- [9] C. Michael and I. Teasdale, *Extracting Glueball Masses From Lattice QCD*, *Nucl. Phys.* **B215** (1983) 433.
- [10] K. Polejaeva and A. Rusetsky, *Three particles in a finite volume*, *Eur. Phys. J.* **A48** (2012) 67, [[arXiv:1203.1241](#)].
- [11] M. T. Hansen and S. R. Sharpe, *Relativistic, model-independent, three-particle quantization condition*, *Phys. Rev.* **D90** (2014), no. 11 116003, [[arXiv:1408.5933](#)].
- [12] M. T. Hansen and S. R. Sharpe, *Expressing the three-particle finite-volume spectrum in terms of the three-to-three scattering amplitude*, [arXiv:1504.04248](#).
- [13] U.-G. Meissner, G. Rios, and A. Rusetsky, *Spectrum of three-body bound states in a finite volume*, *Phys. Rev. Lett.* **114** (2015), no. 9 091602, [[arXiv:1412.4969](#)].
- [14] M. Gockeler, R. Horsley, M. Lage, U. G. Meissner, P. E. L. Rakow, A. Rusetsky, G. Schierholz, and J. M. Zanotti, *Scattering phases for meson and baryon resonances on general moving-frame lattices*, *Phys. Rev.* **D86** (2012) 094513, [[arXiv:1206.4141](#)].
- [15] B. Fahy, J. Bulava, B. Hörz, K. J. Juge, C. Morningstar, and C. H. Wong, *Pion-pion scattering phase shifts with the stochastic LapH method*, *PoS LATTICE2014* (2015) 077, [[arXiv:1410.8843](#)].
- [16] **ETM** Collaboration, C. Helmes, C. Jost, B. Knippschild, C. Liu, J. Liu, L. Liu, C. Urbach, M. Ueding, Z. Wang, and M. Werner, *Hadron-hadron interactions from $N_f = 2 + 1 + 1$ lattice QCD: isospin-2 $\pi\pi$ scattering length*, *JHEP* **09** (2015) 109, [[arXiv:1506.00408](#)].
- [17] D. J. Wilson, R. A. Briceno, J. J. Dudek, R. G. Edwards, and C. E. Thomas, *Coupled $\pi\pi, K\bar{K}$ scattering in P-wave and the ρ resonance from lattice QCD*, [arXiv:1507.02599](#).
- [18] M. Bruno et al., *Simulation of QCD with $N_f = 2 + 1$ flavors of non-perturbatively improved Wilson fermions*, *JHEP* **02** (2015) 043, [[arXiv:1411.3982](#)].
- [19] Lüscher, Martin and Schaefer, Stefan, *Lattice QCD without topology barriers*, *JHEP* **07** (2011) 036, [[arXiv:1105.4749](#)].
- [20] M. Bruno, P. Korcyl, T. Korzec, S. Lottini, and S. Schaefer, *On the extraction of spectral quantities with open boundary conditions*, *PoS LATTICE2014* (2014) 089, [[arXiv:1411.5207](#)].
- [21] C. Morningstar and M. J. Peardon, *Analytic smearing of $SU(3)$ link variables in lattice QCD*, *Phys. Rev.* **D69** (2004) 054501, [[hep-lat/0311018](#)].

- [22] Lüscher, Martin, *Local coherence and deflation of the low quark modes in lattice QCD*, *JHEP* **07** (2007) 081, [[arXiv:0706.2298](#)].
- [23] V. Koch *These proceedings*.
- [24] F. Jegerlehner and A. Nyffeler, *The Muon $g-2$* , *Phys. Rept.* **477** (2009) 1–110, [[arXiv:0902.3360](#)].
- [25] C. Aubin, T. Blum, P. Chau, M. Golterman, S. Peris, and C. Tu, *Finite-volume effects in the hadronic vacuum polarization*, in *Proceedings, 33rd International Symposium on Lattice Field Theory (Lattice 2015)*, 2015. [arXiv:1510.05319](#).
- [26] Lellouch, Laurent and Lüscher, Martin, *Weak transition matrix elements from finite volume correlation functions*, *Commun. Math. Phys.* **219** (2001) 31–44, [[hep-lat/0003023](#)].
- [27] H. B. Meyer, *Lattice QCD and the Timelike Pion Form Factor*, *Phys. Rev. Lett.* **107** (2011) 072002, [[arXiv:1105.1892](#)].
- [28] Briceño, Raúl A. and Hansen, Maxwell T., *Multichannel $0 \rightarrow 2$ and $1 \rightarrow 2$ transition amplitudes for arbitrary spin particles in a finite volume*, *Phys. Rev.* **D92** (2015), no. 7 074509, [[arXiv:1502.04314](#)].
- [29] X. Feng, S. Aoki, S. Hashimoto, and T. Kaneko, *Timelike pion form factor in lattice QCD*, *Phys. Rev.* **D91** (2015), no. 5 054504, [[arXiv:1412.6319](#)].
- [30] R. A. Briceño, J. J. Dudek, R. G. Edwards, C. J. Shultz, C. E. Thomas, and D. J. Wilson, *The resonant $\pi^+\gamma \rightarrow \pi^+\pi^0$ amplitude from Quantum Chromodynamics*, [arXiv:1507.06622](#).
- [31] Lüscher, Martin and Sint, Stefan and Sommer, Rainer and Weisz, Peter, *Chiral symmetry and $O(a)$ improvement in lattice QCD*, *Nucl. Phys.* **B478** (1996) 365–400, [[hep-lat/9605038](#)].
- [32] M. Dalla Brida *These proceedings*.
- [33] S. Aoki, R. Frezzotti, and P. Weisz, *Computation of the improvement coefficient $c(SW)$ to one loop with improved gluon actions*, *Nucl. Phys.* **B540** (1999) 501–519, [[hep-lat/9808007](#)].
- [34] ALPHA Collaboration, J. Bulava, M. Della Morte, J. Heitger, and C. Wittemeier, *Non-perturbative improvement of the axial current in $N_f=3$ lattice QCD with Wilson fermions and tree-level improved gauge action*, *Nucl. Phys.* **B896** (2015) 555–568, [[arXiv:1502.04999](#)].
- [35] A. Francis, B. Jaeger, H. B. Meyer, and H. Wittig, *A new representation of the Adler function for lattice QCD*, *Phys. Rev.* **D88** (2013) 054502, [[arXiv:1306.2532](#)].